Three dimensional four-fermion models - A Monte Carlo study

Stavros Christofi

Frederick Institute of Technology, 1303 Nicosia, Cyprus.

Costas Strouthos

Harvard-MIT (HST) Martinos Center for Biomedical Imaging, Massachusetts General Hospital, Harvard Medical School, Charlestown, MA 02129

Abstract

We present results from numerical simulations of three different $3d$ four-fermion models that exhibit Z_2, $U(1)$, and $SU(2) \times SU(2)$ chiral symmetries, respectively. We performed the simulations by using the hybrid Monte Carlo algorithm. We employed finite size scaling methods on lattices ranging from 8^3 to 40^3 to study the properties of the second order chiral phase transition in each model. The corresponding critical coupling defines an ultraviolet fixed point of the renormalization group. In our high precision simulations, we detected next-to-leading order corrections for various critical exponents and we found them to be in good agreement with existing analytical large-N_f calculations.

1 Introduction

The 3d four-fermion models are among the simplest relativistic quantum field theories of interacting fermions. There are several motivations for studying such models. Dynamical breaking of chiral symmetry occurs at strong enough interaction coupling g_c^2. The chirally broken phase is separated from the chirally symmetric phase by a second order phase transition at the critical coupling. Even though these models are not perturbatively renormalizable, it has been shown that the $1/N_f$ expansion about the fixed point g_c^2 is exactly renormalizable [1]. In addition, four-fermion models are ideal laboratories for studying continuum phase transitions in the presence of massless fermions. Hence, they define new universality classes that are quantitatively different from the ferromagnetic phase transitions in bosonic $O(N)$ Heisenberg spin models. Furthermore, in the framework of $1/N_f$ expansion [2], it has been shown that the universality class of the d-dimensional four-fermion models, where d is between two and four, is the same as the universality class of the Higgs-Yukawa model with the same chiral symmetry. Understanding the properties of the continuum phase transition, which separates the chirally symmetric from the chirally broken phase, requires non-perturbative techniques such as the large-N_f expansion [1, 3, 4, 5, 6, 7, 8, 9, 10], exact renormalization group equations [11, 12], and lattice Monte Carlo simulations [4, 13, 14].

Given that $3d$ four-fermion models incorporate certain important features of QCD, they have been used recently as model field theories to study the properties of the strong interaction at non-zero temperature and non-zero quark number density [15]. In addition, there may be applications of four-fermion models to high-T_c superconductivity [16], for instance in describing non-Fermi liquid behavior in the normal phase [17].

In this paper, we study numerically the critical properties of the $3d$ four-fermion models that exhibit the three different Z_2, abelian $U(1)$, and non-abelian $SU(2) \times SU(2)$ chiral symmetries. In our simulations, we fixed the number of fermion flavors to $N_f = 4$. Our simulations are the first accurate finite size scaling (FSS) studies of the $U(1)$ and $SU(2) \times SU(2)$ models that allow us to detect next-

to-leading order corrections on the values of the critical exponents and to compare them with existing analytical large-N_f predictions. Our results from the Z_2 model simulations are also in good agreement with existing large-N_f predictions as are other accurate Monte Carlo results with $N_f = 2$ [13].

2 Models and Observables

In this section, we introduce the three different versions of the model we shall be dealing with in the bulk of this paper and the observables used to measure the critical exponents of the continuous phase transitions. In the literature, the models are often called the Gross-Neveu models and their continuum space-time lagrangians (we work in Euclidean space) are as follows:

$$\mathcal{L}_A = \bar{\Psi}_i(\partial\!\!\!/ + m)\Psi_i - \frac{g^2}{2N_f}(\bar{\Psi}_i\Psi_i)^2 \tag{1}$$

$$\mathcal{L}_B = \bar{\Psi}_i(\partial\!\!\!/ + m)\Psi_i - \frac{g^2}{2N_f}[(\bar{\Psi}_i\Psi_i)^2 - (\bar{\Psi}_i\gamma_5\Psi_i)^2]. \tag{2}$$

$$\mathcal{L}_C = \bar{\Psi}(\partial\!\!\!/ + m)\Psi - \frac{g^2}{2}\left[(\bar{\Psi}\Psi)^2 - (\bar{\Psi}\gamma_5\vec{\tau}\Psi)^2\right]. \tag{3}$$

We treat Ψ_i, $\bar{\Psi}_i$ as four-component Dirac spinors and the index i runs over N_f fermion species. It can be easily shown that in the chiral limit $m \to 0$, $\mathcal{L}_A$ has a Z_2, $\mathcal{L}_B$ a $U(1)$, and $\mathcal{L}_C$ an $SU(2) \times SU(2)$ chiral symmetry.

For analytical and computational purposes, it is useful to introduce auxiliary fields σ and π_i. Hence, the bosonized lagrangians become quadratic in Ψ_i:

$$\mathcal{L}_A = \bar{\Psi}_i(\partial\!\!\!/ + m + \sigma)\Psi_i + \frac{N_f}{2g^2}\sigma^2. \tag{4}$$

$$\mathcal{L}_B = \bar{\Psi}_i(\partial\!\!\!/ + m + \sigma + i\gamma_5\pi)\Psi_i + \frac{N_f}{2g^2}(\sigma^2 + \pi^2) \tag{5}$$

$$\mathcal{L}_C = \overline{\Psi}_i\left(\partial\!\!\!/ + m + \sigma + i\gamma_5\vec{\pi}\cdot\vec{\tau}\right)\Psi_i + \frac{N_c}{2g^2}\left(\sigma^2 + \vec{\pi}\cdot\vec{\pi}\right). \tag{6}$$

For sufficiently strong coupling $g^2 > g_c^2$ the models exhibit spontaneous symmetry breaking implying dynamical generation of a fermion mass. The pion fields π_i become the associated Goldstone bosons.

We used the staggered fermion discretization with the auxiliary fields living on the dual lattice sites to formulate the models in their bosonized form on the lattice. For each case, we used the hybrid Monte Carlo algorithm with $N_f = 4$ fermion flavors to perform numerical simulations exactly. Details concerning the lattice actions and the numerical algorithm can be found in [4, 18, 19].

We work in the chiral limit to study the chiral phase transition of the models. Hence, we choose not to introduce a bare quark mass into the lattice action. Without the benefit of this interaction, the direction of symmetry breaking changes over the course of the simulation such that $\Sigma \equiv \frac{1}{V}\sum_x \sigma(x)$ and $\Pi_i \equiv \frac{1}{V}\sum_x \pi_i(x)$ average to zero over the ensemble. It is in this way that the absence of spontaneous symmetry breaking on a finite lattice is enforced. Another option is to introduce an effective order parameter Φ equal to the magnitude of the vector $\vec{\Phi} \equiv (\Sigma, \vec{\Pi})$. In the thermodynamic limit, $\langle\Phi\rangle$ is equal to the true order parameter $\langle\sigma\rangle$ extrapolated to zero quark mass.

We employ the finite size scaling (FSS) method [20], a well-established tool, to study the critical behavior of the model on lattices available to us. The correlation length ξ on a finite lattice is limited by the size of the system and consequently no true criticality can be observed. The dependence of a given thermodynamic observable, A, on the size L of the box is singular. According to the FSS hypothesis, in the large volume limit, A is given by:

$$A(t, L) = L^{\rho_A/\nu} Q_A(tL^{1/\nu}), \tag{7}$$

where $t \equiv (\beta_c - \beta)/\beta_c$ is the reduced temperature, ν is the exponent of the correlation length, Q_A is a scaling function that is not singular at zero argument, and ρ_A is the critical exponent for the quantity A. Using eq. (7), one can determine such exponents by measuring A for different values of L.

In the large L limit, the FSS scaling form of the effective order parameter $\langle\Phi\rangle$ is given by

$$\langle\Phi\rangle = L^{-\beta_m/\nu} f_\sigma(tL^{1/\nu}). \tag{8}$$

A standard method to measure the inverse critical coupling $\beta_c \equiv 1/g^2$ for a second order transition is to compute the Binder cumulant $U_B(\beta, L)$ [21], defined by

$$U_B \equiv 1 - \frac{1}{3}\frac{\langle \Phi^4 \rangle}{\langle \Phi^2 \rangle^2}, \tag{9}$$

for various system sizes. Near the critical coupling and on sufficiently large lattices, where subleading corrections from the finite lattice size L are negligible, $U_B = f_B L(tL^{1/\nu})$. Therefore, at β_c, U_B becomes independent of L. Deviations from this relation can be explained by finite size confluent corrections. The leading L_1/L dependence in the deviation of the intersection point β_* from the critical point β_c is estimated by Binder [21] as

$$\frac{1}{\beta_*(L)} = \frac{1}{\beta_c} + \frac{a}{\ln(L_1/L)}. \tag{10}$$

In our analysis we chose L to be the smallest lattice size $L = 8$ and hence L_1 are the remaining lattice sizes.

For the general $O(n)$-symmetric models, it can be easily shown [22] that as the lattice volume tends to infinity in the weak coupling limit, Gaussian fluctuations around $\vec{\Phi} = 0$ lead to $U_B \to 2(n-1)/3n$. For $n = 1$ ($O(1) \equiv Z_2$ symmetry) this gives a zero reference point, for $n = 2$ ($O(2) \equiv U(1)$ symmetry) $U_B \to 1/3$, and for $n = 4$ ($O(4) \equiv SU(2) \times SU(2)$ symmetry) $U_B \to 1/2$. In the chirally broken phase $U_B \to 2/3$ for all n in the thermodynamic limit.

Another quantity of interest is the susceptibility χ that is given, in the static limit of the fluctuation-dissipation theorem, by

$$\chi = \lim_{L\to\infty} V[\langle \vec{\Phi}^2 \rangle - \langle \vec{\Phi} \rangle \cdot \langle \vec{\Phi} \rangle], \tag{11}$$

where V is the lattice volume. For finite systems, the true order parameter $\langle \vec{\Phi} \rangle$ vanishes and for $\beta \geq \beta_c$ the susceptibility is given by:

$$\chi = V\langle \Phi^2 \rangle. \tag{12}$$

This observable should scale at criticality like

$$\chi = L^{\gamma/\nu} f_\chi(tL^{1/\nu}). \tag{13}$$

Furthermore, the logarithmic derivatives of $\langle\Phi\rangle$ can give estimates for the critical exponent ν. It can be easily shown that

$$D \equiv \frac{\partial}{\partial\beta}\ln\langle\Phi\rangle = \left[\frac{\langle\Phi S_b\rangle}{\langle\Phi\rangle} - \langle S_b\rangle\right], \tag{14}$$

where S_b is the bosonic part of the lattice action that is multiplied by the coupling β. D has a scaling relation

$$D = L^{1/\nu} f_D(tL^{1/\nu}). \tag{15}$$

We used the histogram reweighting method [23] to perform our study most effectively. This enabled us to calculate the observables in a region of couplings around the simulation coupling. We utilized this technique efficiently by performing simulations at slightly different couplings β_i close to the critical coupling β_c.

3 Results

In this section we present the results of the data analysis for the three different models. In all three cases, the fermion species number is fixed at $N_f = 4$. An accurate determination of the critical exponents requires a precise determination of the critical coupling. We calculated the critical couplings by using the Binder cumulant technique described in the previous section. For different lattice sizes, the curves $U_B = U_B(\beta)$ should intersect at $\beta = \beta_c$ up to finite size corrections that are visible on the smaller lattices. We used the histogram reweighting method to obtain the values of U_B versus β. We show these values for the Z_2 model in Fig. 1.

We performed the simulations on the largest 40^3 lattice at a single value of the coupling $\beta = 0.835$ and we generated approximately half a million configurations with average trajectory length equal to 1.0. We performed the simulations on the other lattices ($8^3, 12^3, 16^3, 22^3, 30^3$) at all values $\beta = 0.82, 0.83, 0.84, 0.85$ with approximately half to one million configurations for each β. It is clear that in the Z_2 model, the U_B curves intersect at $(\beta_c, U_B(\beta_c)) = (0.835(1), 0.232(8))$.

As expected, the situation is somewhat different in the $U(1)$ model. In this model infrared fluctuations are stronger than in the discrete symmetry model. As

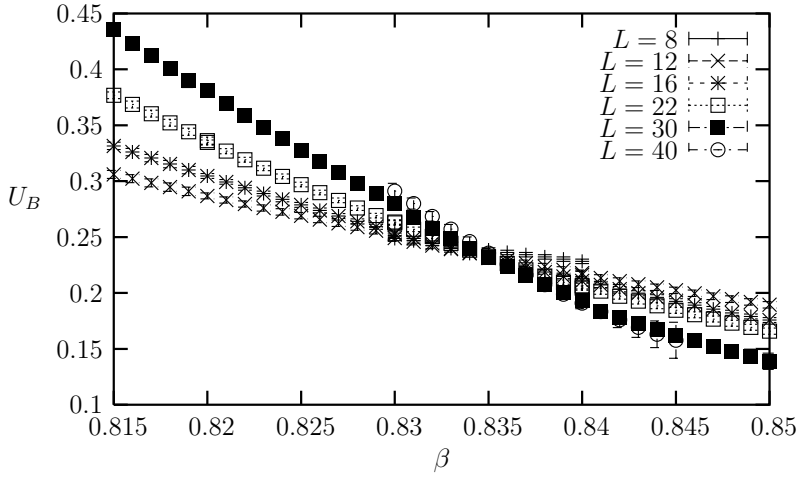

Figure 1: Binder cumulant vs. β for different lattice sizes; Z_2 model.

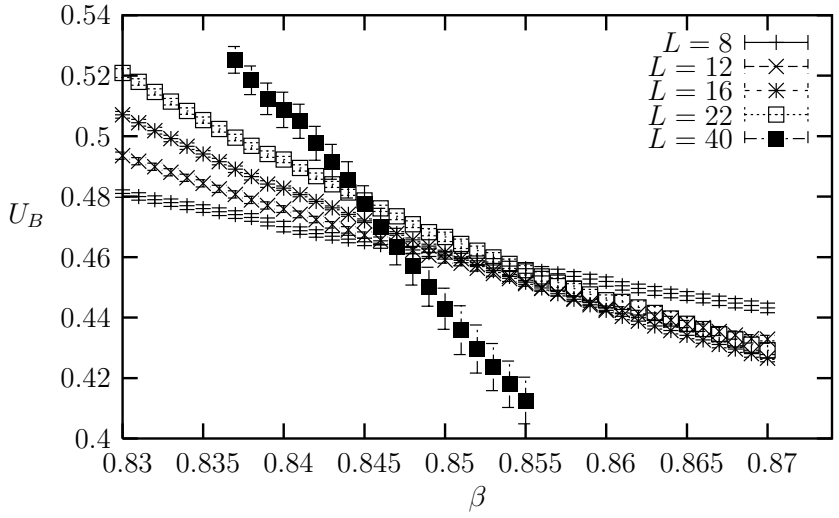

Figure 2: Binder cumulant vs. β for different lattice sizes; $U(1)$ model.

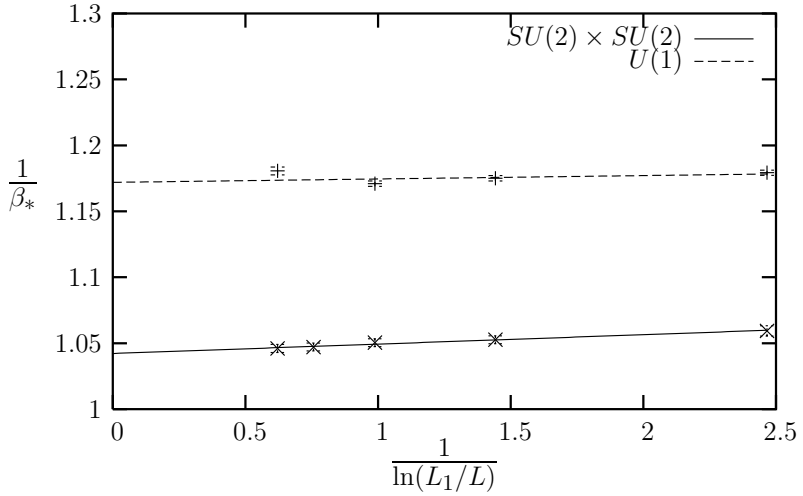

Figure 3: The intersection of $U_B(L)$ and $U_B(L_1)$ for $L = 8$ vs. $\ln(L_1/L)$.

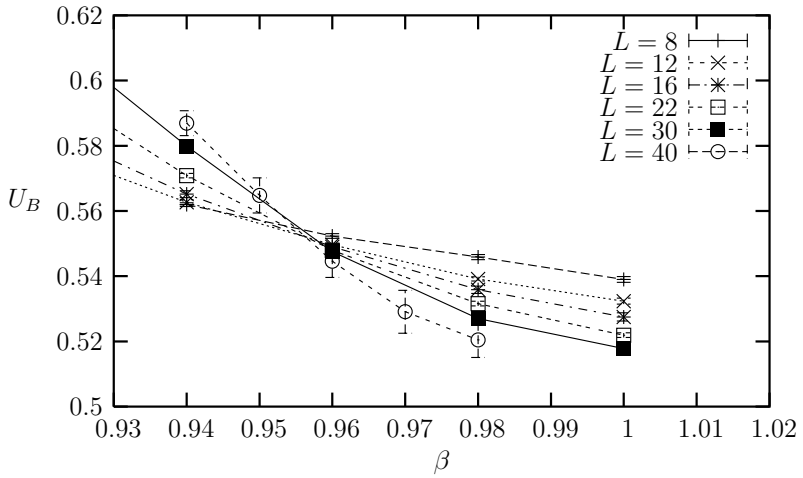

Figure 4: Binder cumulant vs. β for different lattice sizes; $SU(2) \times SU(2)$ model.

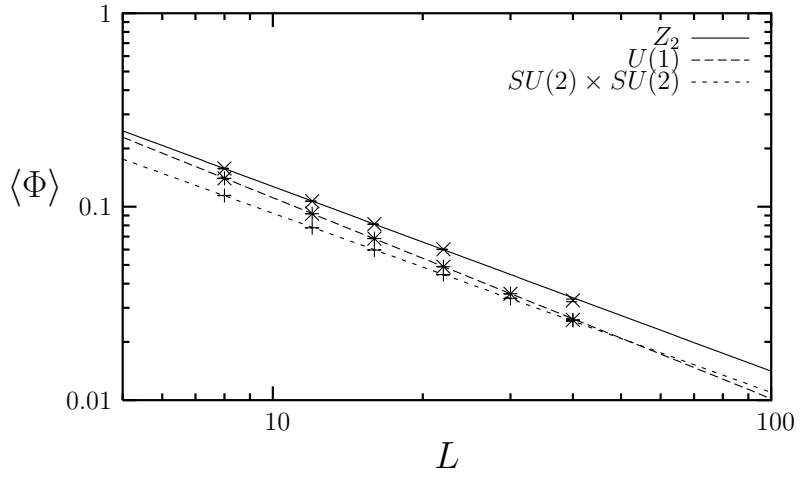

Figure 5: Effective order parameter $\langle\Phi\rangle$ as a function of the lattice size L for all three models.

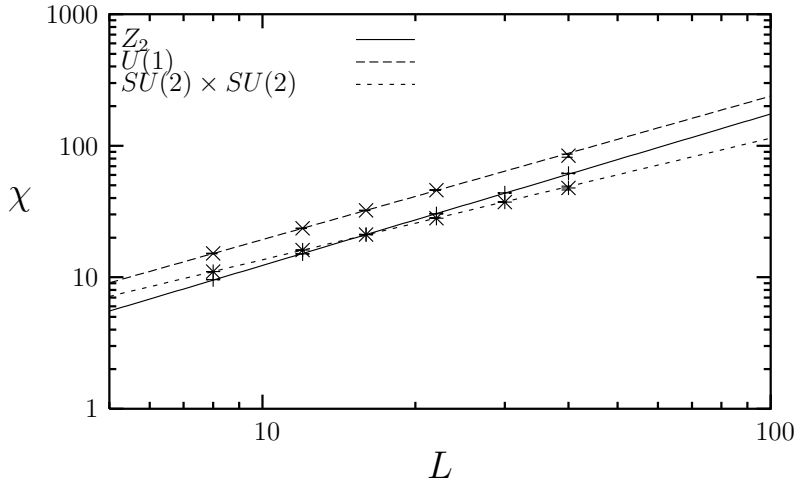

Figure 6: Susceptibility χ as a function of the lattice size L for all three models.

a result, finite size effects near the critical coupling are larger for $U(1)$ than for Z_2. We performed the simulations for the $U(1)$ model on the 40^3 lattices at all values $\beta = 0.830, 0.835, 0.840, 0.845, 0.850, 0.86$, whereas on the smaller lattices at all values $\beta = 0.83, ..., 0.86$ and in steps of 0.01. The data set generated on 30^3 at $\beta = 0.850$ was corrupted and it was not included in the analysis. Approximately 6×10^5 - 1.3×10^6 configurations were generated at each β. We show the values of U_B versus β in Fig. 2. The leading L_1/L finite size corrections are taken into consideration by using eq. (10). We plot $(1/\ln(L_1/L), 1/\beta_*)$ for $L = 8$ in Fig. 3. We computed the errors for $1/\beta_*$ from the jacknife errors for $U_B(\beta)$. The extrapolation of $\frac{1}{\beta_*(L)}$ to the point $1/\ln(L_1/L) = 0$ gives $\beta_c = 0.853(2)$ and $U_B(\beta_c) = 0.424(8)$ on the 40^3 lattice.

We performed an analysis for $SU(2) \times SU(2)$ similar to the one for the $U(1)$ model. In this case, we performed simulations at $\beta = 0.92, ..., 1.00$ in steps of 0.02 for the $8^3, 12^3, 16^3, 22^3, 30^3$ lattices and at $\beta = 0.94, ..., 0.98$ in steps of 0.01 on the largest 40^3 lattice. The curves U_B versus β obtained from histogram reweighting at two consecutive values of β did not intersect. Therefore, to obtain the intersection we used a linear approximation in the middle region between two curves. The values of U_B on different lattices near β_c are shown in Fig. 4 and the extrapolation of $1/\beta_*$ to the point $1/\ln(L_1/L) = 0$ are shown in Fig. 3. We extracted from this analysis the values $\beta_c = 0.960(3)$ and $U(\beta_c) = 0.0.544(7)$ on the largest 40^3 lattice.

Next, we calculated the exponent ratios β_m/ν for the three models by fitting to eq. (8) the values of $\langle \Phi \rangle$ at β_c obtained on different lattice sizes. We obtained $\beta_m/\nu = 0.927(15)$ for Z_2, $\beta_m/\nu = 0.955(20)$ for $U(1)$, and $\beta_m/\nu = 1.04(2)$ for $SU(2) \times SU(2)$. These values of β_m/ν take into consideration the statistical error in β_c. The data and the fitted functions for the three models are shown in Fig. 5.

Similarly, we obtained the exponent ratios γ/ν by fitting the data for the susceptibility χ (eq. (12)) at β_c to its FSS relation eq. (13). We present our results in Table 1 together with analytical predictions obtained from large-N_f calcultations to order $1/N_f^2$ [6, 8]. It is clear that our numerical results are in good agreement with the analytical predictions.

We used the logarithmic derivative D, defined in eq. (14), to calculate the exponent ν. According to eq. (15), at β_c, $D \sim L^{1/\nu}$. The data and the fitting functions for the three models at their critical couplings are shown in fig. 7. We present the values of ν for each model in Table 2 together with the respective values obtained from large-N_f calculations to order $1/N_f^2$ [7, 9, 10]. As in the γ/ν case, the results obtained from our simulations are in good agreement with the analytical predictions.

Using our results for β_m/ν and γ/ν, we can check whether the hyperscaling relation

$$\frac{\beta_m}{\nu} + \frac{1}{2}\frac{\gamma}{\nu} - \frac{d}{2} = 0 \tag{16}$$

is satisfied. We find that for all three different models the left hand side of eq. (16) is consistent with the value zero with an uncertainty $3 - 4\%$.

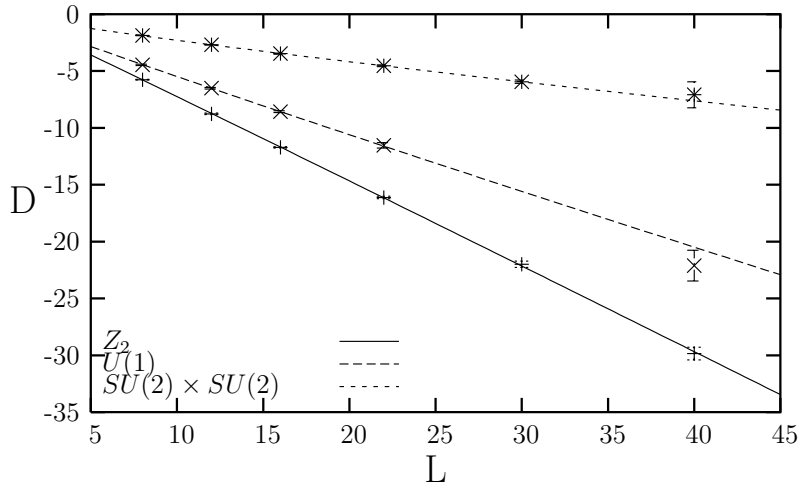

Figure 7: Logarithmic derivarive of the order parameter D as a function of the lattice size L for all three models.

Table 1: Values of γ/ν measured from our simulations and from large-N_f calculations.

	Z_2	$U(1)$	$SU(2) \times SU(2)$
simulations	1.15(25)	1.09(3)	0.925(25)
large N_f [6, 8]	1.132	1.055	0.946

Table 2: Values ν measured from our simulations and from large-N_f calculations.

	Z_2	$U(1)$	$SU(2) \times SU(2)$
simulations	0.98(2)	1.05(2)	1.14(3)
large N_f [7, 9, 10]	0.982	1.015	1.109

4 Conclusions

We presented results from Monte Carlo simulations of $3d$ four-fermion models with Z_2, $U(1)$, and $SU(2) \times SU(2)$ chiral symmetries. These models are among the simplest relativistic field theories of interacting fermions, and therefore are benchmarks for studying critical phenomena in the presence of massless fermions. They are also used as model field theories to study the behavior of strong interaction under extreme conditions and have applications in condensed matter systems. In all three cases, we performed simulations with $N_f = 4$ fermion species. Analytical calculations predict small next-to-leading order corrections for the critical exponents of the second order phase transitions of these models at this intermediate value of N_f. We detected these corrections in our simulations by employing standard finite size scaling techniques and we found them to be in good agreement with large-N_f expansions up to $O(1/N_f^2)$ [6, 7, 8, 9, 10].

Acknowledgements

The simulations were performed on a cluster of 64-bit AMD Opterons 250 at the Frederick Institute of Technology, Cyprus. Discussions with John Gracey and Simon Hands are greatly appreciated.

References

[1] B. Rosenstein, B.J. Warr, and S.H. Park, Phys. Rev. Lett. **62**, 1433 (1989).

[2] J. Zinn-Justin, Nucl. Phys. B **367** 105 (1991).

[3] B. Rosenstein, B.J. Warr, and S.H. Park, Phys. Rep. **205**, 59 (1991).

[4] S. Hands, A. Kocić, J.B. Kogut, An. Phys. **224**, 29 (1993).

[5] S.E. Derkachov, N.A. Kivel, A.S. Stepanko, and A.N. Vasil'ev, Theor. Math. Phys. **22**, 1047 (1992).

[6] J.A. Gracey, Z. Phys. C **59**, 243 (1993).

[7] J.A. Gracey, Int. J. Mod. Phys. A **9**, 567 (1994).

[8] J.A. Gracey, Phys. Lett. B **308**, 65 (1993).

[9] J.A. Gracey, Phys. Rev. D **50**, 2840 (1994).

[10] J.A. Gracey, Z. Phys. C **61**, 115 (1994).

[11] L. Rosa, P. Vitale, and C. Wetterich, Phys. Rev. Lett. **86**, 958 (2001).

[12] F. Hofling, C. Nowak, and C. Wetterich, Phys. Rev. D **66** 205111 (2002).

[13] L. Karkkainen, R. Lacaze, P. Lacock, and B. Peterson, Nucl. Phys. B **415**, 781 (1994).

[14] E. Focht, J. Jersak, and J. Paul, Phys. Rev. D **53** 4616 (1996).

[15] K.G. Klimenko, Z. Phys. **C37**, 457 (1988); B. Rosenstein, B.J. Warr and S.H. Park, Phys. Rev. **D39**, 3088 (1989); S.J. Hands, A. Kocić and J.B. Kogut, Nucl. Phys. **B390**, 355 (1993); J.B. Kogut, M.A. Stephanov and C.G. Strouthos, Phys. Rev. **D58**:096001 (1998); S. Chandrasekharan, J. Cox, K. Holland and U.J. Wiese, Nucl. Phys. B **576** 481 (2000); C.G. Strouthos and S. Christofi, JHEP **0501**:057 2005. J.B. Kogut and C.G. Strouthos, Phys.

Rev. **D63**:054502 (2001); S.J. Hands, B. Lucini and S.E. Morrison, Phys. Rev. **D65**:036004 (2002).

[16] R. Sharkar, Phys. Rev. Lett. **63**, 203 (1989); N. Dorey and N.E. Mavromatos, Phys. Lett. B **250**, 107 (1990); Nucl. Phys. B **386**, 614 (1992).

[17] I.J.R. Aitchison and N.E. Mavromatos, Phys. Rev. B**53**, 9321 (1996).

[18] S.J. Hands, S. Kim and J.B. Kogut, Nucl. Phys. B **442**, 364 (1995).

[19] S.J. Hands and S.E. Morrison, Phys. Rev. D **59**, 116002 (1999).

[20] M.N. Barber, in *Phase Transitions and Critical Phenomena*, edited by C. Domb and J. Lebowitz (Academic, New York, 1983).

[21] K. Binder, Z. Phys. B **43**, 119 (1981).

[22] C. Holm and W. Janke, Phys. Rev. B **48**, 936 (1993).

[23] A.M. Ferrenberg and R.H. Swendsen, Phys. Rev. Lett. **61**, 2635 (1988).